

Efficient method for estimation of fission fragment yields of r -process nuclei

Jhilam Sadhukhan,^{1,2} Samuel A. Giuliani,³ Zachary Matheson,³ and Witold Nazarewicz⁴

¹*Physics Group, Variable Energy Cyclotron Centre, 1/AF Bidhan Nagar, Kolkata 700064, India*

²*Homi Bhabha National Institute, Anushakti Nagar, Mumbai 400094, India*

³*FRIB Laboratory, Michigan State University, East Lansing, Michigan 48824, USA*

⁴*Department of Physics and Astronomy and FRIB Laboratory, Michigan State University, East Lansing, Michigan 48824, USA*

Background: More than half of all the elements heavier than iron are made by the rapid neutron capture process (or r process). For very neutron-rich astrophysical conditions, such as those found in the tidal ejecta of neutron stars, nuclear fission determines the r -process endpoint, and the fission fragment yields shape the final abundances of $110 \leq A \leq 170$ nuclei. The knowledge of fission fragment yields of hundreds of nuclei inhabiting very neutron-rich regions of the nuclear landscape is thus crucial for the modeling of heavy-element nucleosynthesis.

Purpose: In this study, we propose a model for the fast calculation of fission fragment yields based on the concept of shell-stabilized prefragments defined with help of the nucleonic localization functions.

Methods: To generate realistic potential energy surfaces and nucleonic localizations, we apply Skyrme Density Functional Theory. The distribution of the neck nucleons among the two prefragments is obtained by means of a statistical model.

Results: We benchmark the method by studying the fission yields of ^{178}Pt , ^{240}Pu , ^{254}Cf , and $^{254,256,258}\text{Fm}$ and show that it satisfactorily explains the experimental data. We then make predictions for ^{254}Pu and ^{290}Fm as two representative cases of fissioning nuclei that are expected to significantly contribute during the r -process nucleosynthesis occurring in neutron star mergers.

Conclusions: The proposed framework provides an efficient alternative to microscopic approaches based on the evolution of the system in a space of collective coordinates all the way to scission. It can be used to carry out global calculations of fission fragment distributions across the r -process region.

I. INTRODUCTION

The predictive power of r -process network calculations could be improved by providing sound predictions of fission fragment yields, including yields from spontaneous fission (SF), beta-delayed fission, and neutron-induced fission. In particular, it has been long established that fission fragment distributions play a crucial role in shaping the final r -process abundances [1–6], and recent studies suggest that uncertainties in fission yields should be reduced in order to properly constrain the contribution of binary neutron star mergers to the chemical evolution of r -process elements [7]. When it comes to realistic predictions, the Langevin approach [8–10] has proven to be extremely successful in terms of quantitative reproduction of fragment yields. Unfortunately, full-fledged Langevin calculations in a multidimensional collective space, based on the microscopic nuclear density functional theory (DFT) input, are computationally expensive when it comes to large-scale theoretical fission surveys. The same is true for the time-dependent calculations [11–16] based on self-consistent approaches. Given the computational cost of microscopic methods and the large number of fissioning nuclei that are expected to contribute during the r -process nucleosynthesis, network calculations have mostly relied on simple parametrizations or highly phenomenological models to determine fission yields.

To date, the models that aim at global surveys of fission yields can be grouped into three main categories [17]. The first group comprises the so-called Brownian

motion models, wherein the fission process is described as an overdamped motion across potential energy surfaces obtained from microscopic-macroscopic calculations [18–20]. These models take into account the dissipative dynamics required to describe the full distribution of fission yields. To deduce charge yields, additional assumptions are made such as a linear scaling of mass distributions.

Methods belonging to the second category, the scission-point models [21–23], are free from this limitation because they treat charge asymmetry as a collective degree of freedom. However, the scission-point approach relies on a static description of the fragments along the scission configuration, thus neglecting fission dynamics. For recent realizations of this model, see, e.g., Refs. [24–27]. Within this category, another simplified static description is the random neck-rupture model [28, 29] where the location of the neck is decided randomly following an appropriate statistical weight.

Finally, the third category are semi-empirical models, such as GEF [30] and ABLA [31], which have been widely used in r -process calculations [3–5, 32, 33]. These models turned out to be extremely successful in describing data close to stability, since their parameters have been fine-tuned to reproduce observed fission fragments distributions. However, their applicability to extrapolate far from stability is questionable and the related uncertainties are difficult to assess.

To overcome these shortcomings, the present paper presents an efficient and predictive model for fission fragment yields that is based on the microscopic DFT input. There are two main assumptions behind our model: (i)

the formation of fission fragments is governed mainly by shell effects of the prefragments that develop in the pre-scission region; and (ii) the final fragments are produced in the scission region by a rapid distribution of neck nucleons, a process that is statistical in nature. Both assumptions are based on results of previous microscopic calculations [8, 34, 35]. Indeed, by studying the nucleonic localization function (NLF) for deformed configurations of fissioning nuclei, we observe that two distinct prefragments form and then separate well before scission is reached. This early development of the prefragments is a manifestation of the freeze-out of single particle energies along the fission path [36–39] as the system tries to maintain its microscopic configuration to avoid level crossings. The suggestion that the prefragment particle numbers play essential roles in determining the fission fragment distribution can be traced back to strong shell effects in prefragments in the semiclassical periodic-orbit theory [40, 41].

Within the proposed model, it is not necessary to calculate the full potential energy surface (PES) up to the scission configuration, since a simplified estimation of the PES is sufficient to obtain the most-probable prefragment configuration(s). Then, final fragment yields are generated by distributing the neck nucleons into prefragments according to a statistical prescription wherein the frequency of a particular fragmentation channel is decided with an appropriate microcanonical probability [21, 42].

The paper is organized as follows. Our model is described in Sec. II. Section III contains the benchmark calculations of fission yields and presents results for two representative cases of r -process nuclei. Section IV contains a summary and conclusions.

II. THEORETICAL FRAMEWORK

A. Selection of configurations to calculate NLFs

Our method of estimating primary fission yields is based on NLFs computed at a point on the most probable fission path that corresponds to a compact configuration at the outer turning point well before scission. This configuration, obtained by minimizing the collective action between the ground state and the outer turning line, determines the peak position of the fragment yield distribution. Specifically, for a given nucleus and fission decay (spontaneous, neutron-induced or fusion-fission) we find the point where the total energy drops down from the fission barrier to its ground state value (E_{GS}) along the most-probable fission path. In case of SF, this point lies on the outer turning line. For this configuration, called C in the following, the two *prefragments* are identified using nucleonic densities and NLFs. As discussed earlier, NLFs are related to the underlying shell structure and remain almost unaffected along an effective fission path [34, 43, 44]. If several fission pathways are close in energy (multimodal fission) [45], multiple nuclear

configurations may contribute to the yield distribution. For example, both mass-symmetric and mass-asymmetric structures must be accounted for when the corresponding fission valleys are close.

The microscopic DFT input has been generated by using the HFB solver HFODD [46]. In this study, we applied two Skyrme energy density functionals (EDFs) in the particle-hole channel: SkM* [47] and UNEDF1_{HFB} [48]. In the pairing channel, we took the mixed-type density-dependent delta interaction [49]. For neutron-induced fission, the PES is obtained using the finite-temperature Hartree-Fock-Bogoliubov (HFB) formalism, in which the compound nucleus is described using the grand-canonical ensemble [50–52].

B. Definition of prefragments from NLF

NLF measures the probability of finding two nucleons with the same spin σ and isospin q at the same spatial localization. In this work, it is computed as described in Refs. [53, 54]:

$$C_{q\sigma} = \left[1 + \left(\frac{\tau_{q\sigma}\rho_{q\sigma} - \frac{1}{4}|\nabla\rho_{q\sigma}|^2 - \mathbf{j}_{q\sigma}^2}{\rho_{q\sigma}\tau_{q\sigma}^{\text{TF}}} \right)^2 \right]^{-1}, \quad (1)$$

where $\rho_{q\sigma}$, $\tau_{q\sigma}$, $\mathbf{j}_{q\sigma}$ and $\nabla\rho_{q\sigma}$ are the particle density, kinetic energy density, current density, and density gradient, respectively. The Thomas-Fermi kinetic energy density $\tau_{q\sigma}^{\text{TF}} = \frac{3}{5}(6\pi^2)^{2/3}\rho_{q\sigma}^{5/3}$ is introduced as a normalization parameter.

Figure 1 shows the NLFs used in the calculation of spontaneous fission (SF) yields in the selected nuclei. We recall that a value of $C \sim 1$ indicates a large nucleon's localization, i.e., a low probability of finding two nucleons with the same spin and isospin at the same spatial localization. On the other hand, $C = 1/2$ corresponds to a limit of an homogeneous Fermi gas.

The prefragments are determined using the following algorithm. Along the nuclear symmetry axis, we identify the center of the prefragment as the NLF maximum (or minimum) placed at the center of the NLF's concentric shell rings as shown in Fig. 1. In this way, the equatorial plane passing through this center delimits the prefragment's hemisphere. Proton and neutron numbers of prefragments are obtained by integrating the nucleon density over such hemispheres and doubling the resulting number. This method is a generalization of the previous definition [34]. As evident from Fig. 1 and discussed below, in most of fissioning actinide nuclei, one of the prefragments is spherical due to the shell structure of the doubly-magic nucleus ^{132}Sn , while the other has an elongated shape with two local NLF maxima separated by the central minimum.

Thus, a deformed fissioning nucleus can be thought of as two well-formed prefragments connected by a “glue” of nucleons in the neck. This concept is illustrated in

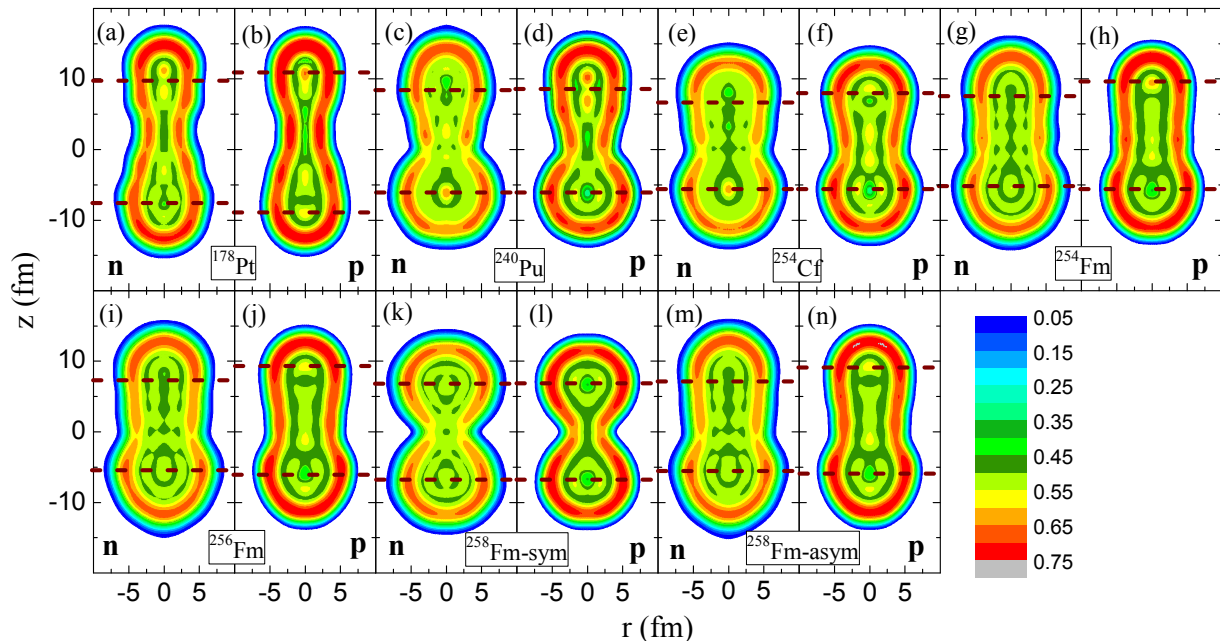


FIG. 1. NLFs of selected nuclei used in the calculation of spontaneous fission fragment yield distributions. (a), (b), (g)-(n) are calculated with UNEDF1_{HFB} EDF and (c)-(f) are calculated with SkM* EDF. Dashed lines indicate equatorial planes of the prefragments.

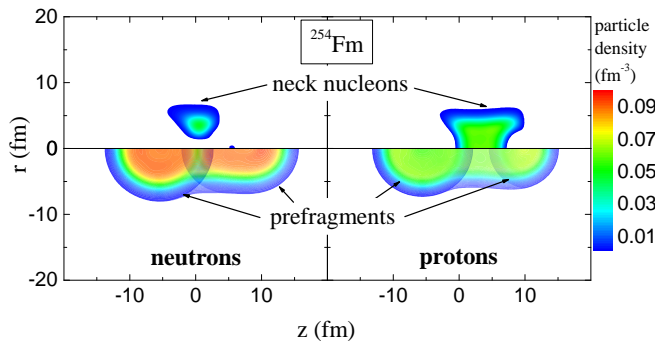


FIG. 2. Density distributions of prefragments (bottom) and neck-nucleons (top) in the configuration C of ^{254}Fm indicated in Fig. 3(a), obtained with UNEDF1_{HFB}.

Fig. 2, which shows the neutron and proton prefragments, and the neck nucleons for the configuration C of ^{254}Fm indicated in Fig. 3(a).

C. Yield distributions from prefragments

In the next step, the neck nucleons are distributed among the two prefragments with all possible combinations sampled. For each combination, binding energies of the resulting *fragments* (E_{b1} for the fragment (A_1, Z_1) and E_{b2} for the fragment (A_2, Z_2)) are calculated using

the isospin-dependent liquid drop model [55] (It is to be noted that the minimum mass and charge of a fragment is that of a corresponding prefragment). We again emphasize that the prefragment configurations are obtained using the most probable fission path calculated using realistic inputs. The liquid drop energy essentially determines the width of the yield distribution which primarily depends on the global isovector properties such as symmetry and Coulomb energies.

The energy of each fragment combination is $E_r = E_t - (E_{b1} + E_{b2} + E_C)$, where E_t is the calculated energy of the fissioning nucleus at C (which is equal to E_{GS}) and E_C is the electrostatic repulsion energy between the fragments. We assumed the charges to be that of two point charges located at the center of mass of the fragments. For completeness, we checked that the correction in the yield distributions due to deformed charge distributions is negligible. Subsequently, each pair of fragments is associated with a microcanonical probability distribution [21]

$$P(A_1, A_2) \propto \sqrt{\left(\frac{(A_1 A_2)^8}{(A_1^{5/3} + A_2^{5/3})^3 (A_1 + A_2)^3} \right) \frac{a_1 a_2}{(a_1 + a_2)^5}} \\ \times \left(1 - \frac{1}{2\sqrt{(a_1 + a_2)E_r}} \right) E_r^{9/4} \exp \left\{ 2\sqrt{(a_1 + a_2)E_r} \right\}, \quad (2)$$

where $a_i = A_i/10 \text{ MeV}^{-1}$ is the level density parameter [8]. Finally, we fold the probabilities with a Gaussian smoothing function of width 3 for A and 2 for Z [8].

To assess the robustness of our calculations, we estimated uncertainties in the yield distributions with re-

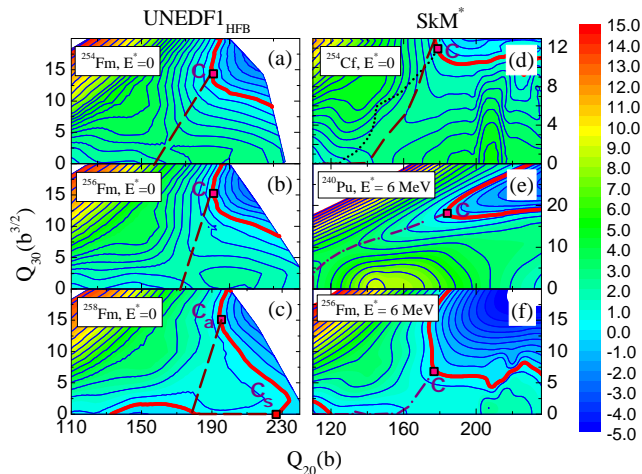


FIG. 3. PESs of $^{254,256,258}\text{Fm}$, ^{254}Cf , and ^{240}Pu calculated with UNEDF1_{HFB} (left panels) and SkM* (right panels). For each nucleus, the energy (in MeV) is normalized to the ground state energy E_{GS} . The contours $E = E_{\text{GS}}$ are indicated by thick solid lines. Most probable fission paths are calculated dynamically for $E^* = 0$ with constant inertia (dashed lines in (a)-(d)) and non-perturbative cranking inertia (dotted line in (d)) while static pathways are computed for $E^* > 0$ (dash-dotted lines in (e) and (f)). The configurations \mathcal{C} used to compute prefragments are marked by squares. For ^{258}Fm , two configurations are shown: \mathcal{C}_s (symmetric fission pathway) and \mathcal{C}_a (asymmetric fission pathway).

spect to the model parameters, including the choice of the EDF. The distributions are found to be very sensitive to the prefragment particle numbers. In general, the neutron and proton numbers of a prefragment are not integers as they are obtained by integrating density distributions. Hence, we consider the nearest integer as average particle (neutron or proton) number with a spread of ± 1 around this average value. This particle number uncertainty is considered for both the prefragments of a fissioning system. The yield distributions are then obtained for all possible combinations among these particle numbers. The resulting uncertainty in the yield distributions is referred to as the two-particle uncertainty. On the other hand, uncertainties from different realizations of the liquid drop model and other parameters defining the microcanonical probability mainly modify the tail part of the distributions and its magnitude is smaller than the prefragment-uncertainty. Also, we checked that the absolute value of E_r weakly affects yield distributions. We conclude therefore that, while a more microscopic treatment of this quantity could be important for estimating observables such as the total kinetic energy of the fragments, its impact on the fragments yields is minor within our model.

III. RESULTS

A. Benchmarking the model against experimental data

To benchmark our model, we consider several nuclei (^{178}Pt , ^{240}Pu , ^{254}Cf , and $^{254,256,258}\text{Fm}$) for which fission yield distributions have been determined experimentally. For each of these systems, an appropriate configuration \mathcal{C} is identified to extract the prefragments. In case of thermal fission (n_{th}, f), we calculate the PES at the thermal excitation energy (≈ 6 MeV) and we select the configuration \mathcal{C} by taking the point on the static fission path that has zero energy with respect to the ground state minimum obtained at $E^* = 6$ MeV. For pre-actinide nuclei such as ^{178}Pt , the potential barrier is fairly flat and broad, and it is crossed by the fusion valley [56, 57]. Therefore, we have arbitrarily chosen a configuration on the static paths of ^{178}Pt [57] at $Q_{20} = 220$ b (UNEDF1_{HFB}) and 190 b (SkM*). We checked that the prefragment structure does not change beyond these points.

The isotopes of Fm are of special interest as the corresponding mass yields show a transition from asymmetric to a symmetric distribution with increasing parent mass [15, 45, 58–60]. Calculated PESs are shown in Fig. 3. For all the systems except ^{258}Fm , fission fragment distributions are expected to be asymmetric because of a large outer fission barrier. However, the potential surface of ^{258}Fm is rather flat at large Q_{20} and we expect contributions from both symmetric and asymmetric fission pathways.

From previous calculations [8, 61, 62], it is found that the topology of the minimum action path is rather simple on the Q_{20} - Q_{30} plane irrespective of the choice of collective inertia. Usually, it follows the minimum distance from a mass-symmetric configuration outside the fission isomer to the nearest outer turning point. This is verified in Fig. 3 where the dynamical paths calculated with constant inertia and non-perturbative cranking inertia [63, 64] are compared for ^{254}Cf . Although there is a local detour inside the barrier due to non-perturbative inertia, both the pathways reach the outer turning line at nearby points at which the NLFs are practically identical. A similar behavior has been reported for the fission paths of ^{240}Pu [8]. Therefore, as we are only concerned with identifying the appropriate \mathcal{C} configuration, we assumed a constant inertia for the calculation of minimum action paths of Fm isotopes and the relative weight of the two-configurations of ^{258}Fm . This reduces the computational burden enormously compared to calculations with non-perturbative collective inertia.

To complement the NLFs shown in Fig. 1, Fig. 4 displays the calculated prefragments for different fissioning systems. We notice that for the actinides the heavy prefragment is very close to the doubly-magic nucleus ^{132}Sn irrespective of the EDF used. This result suggests an early development of shell effects along the fission

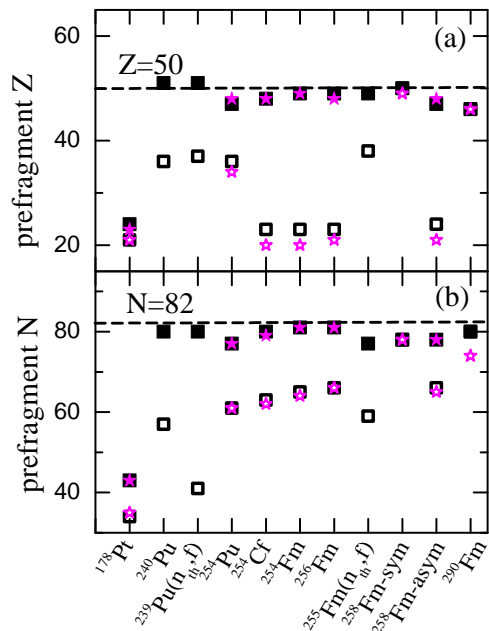


FIG. 4. Prefragments for different fissioning systems calculated with SkM* (squares) and UNEDF1_{HFB} (stars). Top: proton number; bottom: neutron number. Heavy and light prefragments are marked with closed and open symbols, respectively. Note that for C_s configurations of ^{258}Fm and ^{290}Fm only symmetric fission is expected and hence only one symbol is shown.

path, in agreement with the previous NLF-based study on the formation of ^{240}Pu fission fragments [34]. On the other hand, both mass and charge of the lighter fragment are subject to appreciable fluctuations; this supports the need for the microscopic determination of prefragments. As already pointed out in Ref. [34], the main advantage of using NLFs is that the localization patterns of the prefragments defined at the outer turning line closely resemble those at scission. This can be confirmed by the fact that both proton and neutron single particle levels show a smooth pattern in their evolution from the outer turning point to the scission point, indicating the stabilization of shell effects [36–39]. In Fig. 5, we show the single-particle levels of ^{240}Pu along the most-probable effective fission path of Ref. [34]. This plot shows that both neutron and proton energy levels change very gradually maintaining the low single-particle level density around the Fermi level. An additional factor that maintains the adiabaticity of the collective motion is the presence of pairing correlations, which reduce the effect of configuration changes [36, 37, 61, 65, 66].

Since the notion of a prefragment is a purely theoretical concept, their properties cannot be measured experimentally. Moreover, alternate prefragment definitions exist [39, 67]. Consequently, the validity of a prefragment-based description is checked by the ability of a model to predict and reproduce experimental observables. To this

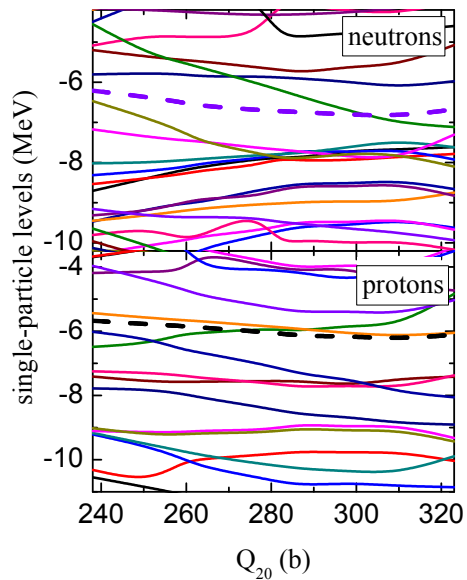


FIG. 5. Single particle levels calculated with SkM* along the most probable fission path of ^{240}Pu from the outer turning point to scission. Fermi energies are indicated by thick dashed lines.

end, in Fig. 6, we benchmark our approach by predicting the fission fragment mass and charge distributions for selected nuclei. In general, very good agreement with experiment has been obtained for SF. For thermal fission, one does not expect a drastic change compared to SF as the excitation energy is quite low. Indeed, for $^{239}\text{Pu}(n_{th}, f)$ both experiment and predictions overlap with the SF fragment yields. For $^{255}\text{Fm}(n_{th}, f)$ we predict broader mass and charge distributions than for SF. We note that the $^{255}\text{Fm}(n_{th}, f)$ experimental data show an asymmetry in the heavy and light fragment yields, which may be attributed to neutron evaporations from the primary fragments. In the case of ^{258}Fm , the mass-symmetric trajectory produces a sharp peak in the SF mass distribution while the asymmetric one contributes to the broad tail, in agreement with the experimental mass distribution. Based on these benchmark calculations, we conclude that the proposed method is robust with respect to the choice of the EDF as the SkM* and UNEDF1_{HFB} results are very close. The information contained in the outer-point configurations \mathcal{C} , supplemented by the statistical treatment of the neck nucleons is sufficient to predict the mass and charge flows, which are governed by macroscopic liquid drop forces.

B. Comparison with Langevin results for ^{294}Og

Our approach to fission fragments distributions is rooted in the microscopic Langevin calculations suggesting a separation of scales between the formation of the prefragments and the rapid rearrangement of the neck

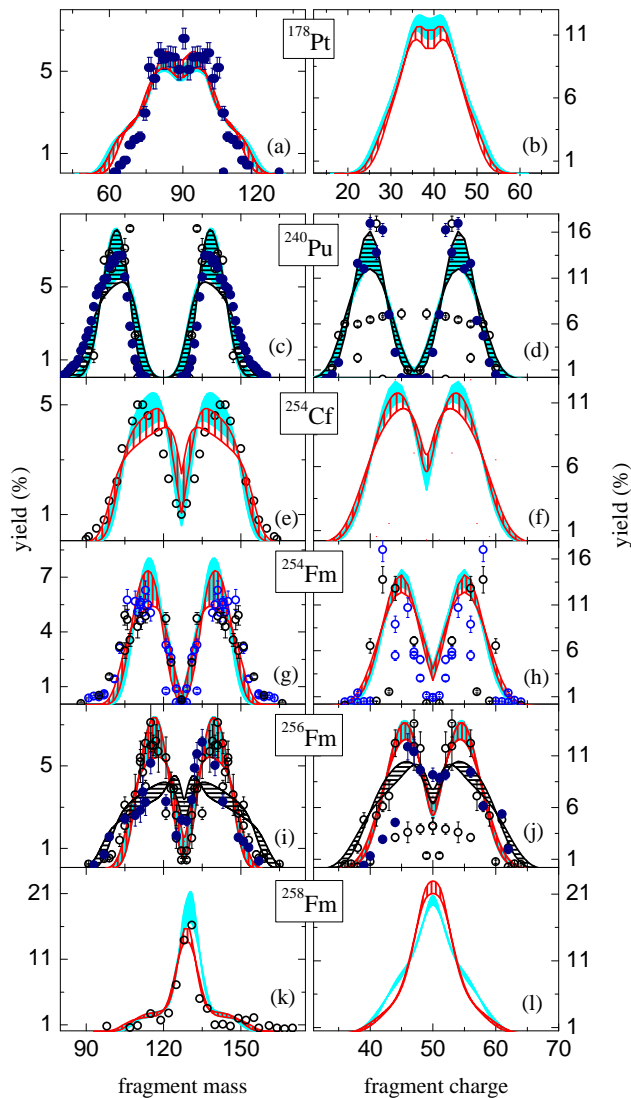


FIG. 6. Calculated yield distributions for SF (shaded for SkM* and vertically patterned for UNEDF1_{HFB}) and thermal fission (horizontally patterned) with two-particle uncertainty in each prefragment. Open circles: experimental data for SF of ^{240}Pu [68], ^{254}Cf [69], ^{254}Fm [70, 71], ^{256}Fm [72], ^{258}Fm [73]; closed circles: experimental data for thermal fission of ^{240}Pu [74] and ^{256}Fm [75], and heavy-ion induced fission of ^{178}Pt [57].

nucleons at scission [8]. To further prove the capability of our model to retain the relevant physics captured by Langevin calculations, Fig. 7 compares the fission fragments distributions for ^{294}Og predicted in our model with those predicted in Ref. [35] using the Langevin approach. Both models are in a fairly good agreement, predicting the emergence of cluster decay (with the heavy fragment centered around ^{208}Pb) as a main fission mode. This again confirms the ability of the present model to capture the relevant physics. We notice that our calculations pre-

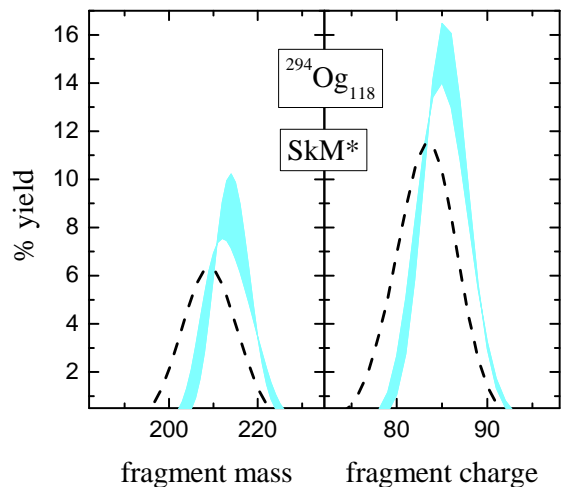


FIG. 7. Yield distributions for ^{294}Og calculated in SkM* using the statistical model described in this work (shaded region) and the Langevin approach of Ref. [35] (dashed lines). Only heavy-fragment distributions are plotted.

dict a slight shift towards a more asymmetric split, and a narrower distribution of yields. Both effects can be related to the lower mass and charge limits imposed by the identification of the prefragments, which drive the final configurations towards a heavier fragment and slightly reduce the fragment phase space.

C. Application to r -process nuclei

Encouraged by the positive outcome of the benchmarking exercise, we extended our calculations to r -process nuclei. To this end, we consider ^{254}Pu as a representative fissioning nucleus that is expected to significantly contribute to the r -process nucleosynthesis occurring in neutron star mergers and the extremely neutron-rich ^{290}Fm nucleus which is speculated to be formed at the edge of r -process [5]. A one-dimensional fission trajectory is calculated for each isotope up to the fission isomer by constraining Q_{20} and leaving the other degrees of freedom unconstrained. In the region between the fission isomer and the outer turning line, the collective space is expanded to include Q_{30} in order to account for mass asymmetry. The resulting PESs and yield distributions are shown in Fig. 8 and Fig. 9 for ^{254}Pu and ^{290}Fm , respectively. These are compared with predictions given by the semi-empirical GEF [30] and ABLA [31] models.

For ^{254}Pu , our method predicts yield distributions somewhere in between the GEF and ABLA results. Distributions are wider as predicted by GEF and also have considerable symmetric contributions as in ABLA. For ^{290}Fm , our approach predicts a symmetric fission centered around ^{145}Sn , but with a wider fragment distribution compared to GEF and closer to the width predicted

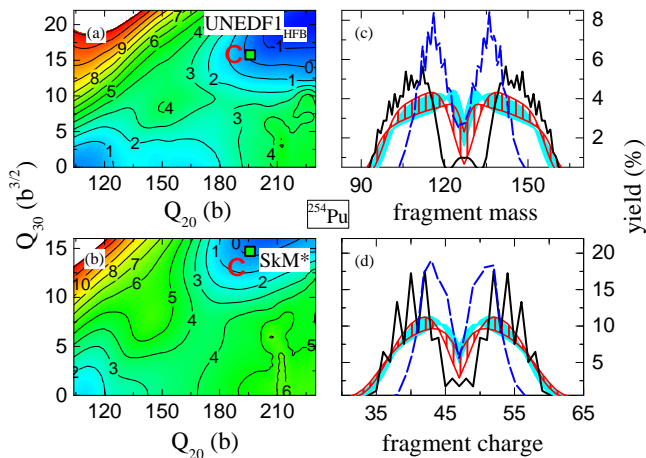


FIG. 8. Predicted fission properties of r -process nucleus ^{254}Pu . Left: Potential energy surfaces calculated with (a) UNEDF1_{HFB} and (b) SkM* functionals. The configurations C are marked by square symbols. Right: Predicted (c) mass and (d) charge yield distributions (shaded and patterned regions for SkM* and UNEDF1_{HFB}, respectively) given by our method. The GEF [30] and ABLA [31] results are shown by solid and dashed lines, respectively.

by the ABLA model. This result suggests a weakening of $Z/N = 50/82$ shell stabilization for very neutron-rich nuclei, in agreement with a general trend found in recent calculations [20] that would extend the range of r -process elements affected by fission cycling [6]. It is worth noting that while in both GEF and ABLA the effect of shell stabilization determining the fission modes is introduced *ad hoc* using parameters finely tuned to reproduce experimental data, in our approach they naturally emerge from the underlying EDF. This is a crucial feature for the studies of exotic rare isotopes whose shell closures may differ from those found in nuclei close to the line of beta stability. Finally, we point out the extreme robustness of the fission yields with respect to the choice of EDF even in this region far from stability. This feature, which has been also found in our DFT+Langevin studies [35], gives us the confidence to extend our study to systematic calculations or r -process nuclei.

IV. CONCLUSIONS

We developed a method for estimating fission fragment yields based on nuclear DFT with realistic energy density functionals and simple statistical assumptions governing the redistribution of neck nucleons at scission. This method is inspired by recent microscopic Langevin calculations suggesting an early formation of the prefragments along effective fission paths and a rapid distribution of

neck nucleons around the scission point [34], which is reminiscent of the separability principle proposed in previous phenomenological studies [76]. The new approach

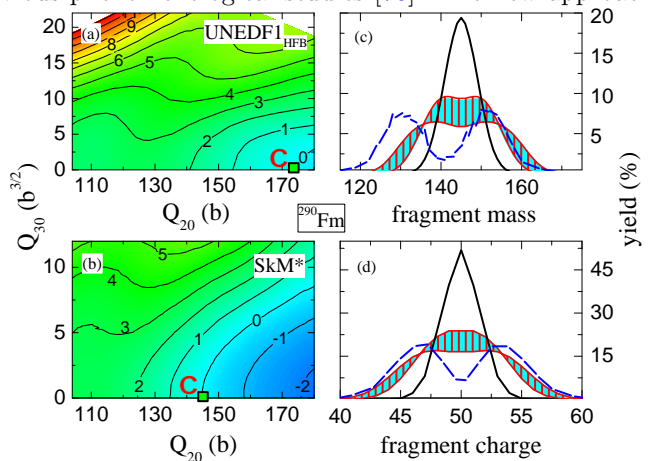


FIG. 9. Similar as in Fig. 8 but for ^{290}Fm . The predictions of UNEDF1_{HFB} and SkM* are practically identical.

is computationally inexpensive compared to more microscopic models that require the knowledge of the full multi-dimensional PES and related quantities (such as the collective inertia) all the way to scission, while retaining the relevant physics determining the structure of fission fragment distributions. A sound agreement with experimental charge and mass distributions is obtained for a wide range of fissioning nuclei.

In the next step, we intend to use the new method to carry out global calculations of fission fragment distributions across the r -process region. Such input could be combined with systematic calculations of fission rates [77–80] to consistently study the impact of fission on the r -process nucleosynthesis. Moreover, the present formulation of the model, based on DFT computation of densities in even-even nuclei, is not capable of reproducing the even-odd effects of fission fragment yields [81]. We will consider this aspect in our future studies.

ACKNOWLEDGMENTS

The authors are grateful to G. Martínez Pinedo and N. Vassh for providing the ABLA and GEF data, respectively, used in Figs. 8 and 9. This work was supported by the U.S. Department of Energy under Award Numbers DE-NA0003885 (NNSA, the Stewardship Science Academic Alliances program), DE-SC0013365 (Office of Science), and DE-SC0018083 (Office of Science, NUCLEI SciDAC-4 collaboration). Computing support came from the Lawrence Livermore National Laboratory (LLNL) Institutional Computing Grand Challenge program.

- [1] C. J. Horowitz, A. Arcones, B. Côté, I. Dillmann, W. Nazarewicz, I. U. Roederer, H. Schatz, A. Aprahamian, D. Atanasov, A. Bauswein, T. C. Beers, J. Bliss, M. Brodeur, J. A. Clark, A. Frebel, F. Foucart, C. J. Hansen, O. Just, A. Kankainen, G. C. McLaughlin, J. M. Kelly, S. N. Liddick, D. M. Lee, J. Lippuner, D. Martin, J. Mendoza-Temis, B. D. Metzger, M. R. Mumpower, G. Perdikakis, J. Pereira, B. W. O’Shea, R. Reifarh, A. M. Rogers, D. M. Siegel, A. Spyrou, R. Surman, X. Tang, T. Uesaka, and M. Wang, “r-process nucleosynthesis: connecting rare-isotope beam facilities with the cosmos,” *J. Phys. G* **46**, 083001 (2019).
- [2] S. Goriely, J.-L. Sida, J.-F. Lemaître, S. Panebianco, N. Dubray, S. Hilaire, A. Bauswein, and H.-T. Janka, “New fission fragment distributions and r-process origin of the rare-earth elements,” *Phys. Rev. Lett.* **111**, 242502 (2013).
- [3] M. Eichler, A. Arcones, A. Kelic, O. Korobkin, K. Langanke, T. Marketin, G. Martinez-Pinedo, I. Panov, T. Rauscher, S. Rosswog, C. Winteler, N. T. Zinner, and F.-K. Thielemann, “The role of fission in neutron star mergers and its impact on the r-process peaks,” *Astrophys. J.* **808**, 30 (2015).
- [4] S. Goriely, “The fundamental role of fission during r-process nucleosynthesis in neutron star mergers,” *Eur. Phys. J. A* **51**, 22 (2015).
- [5] N. Vassh, R. Vogt, R. Surman, J. Randrup, T. M. Sprouse, M. R. Mumpower, P. Jaffke, D. Shaw, E. M. Holmbeck, Y.-L. Zhu, and G. C. McLaughlin, “Using excitation-energy dependent fission yields to identify key fissioning nuclei in r -process nucleosynthesis,” *J. Phys. G* **46**, 065202 (2019).
- [6] N. Vassh, M. R. Mumpower, G. C. McLaughlin, T. M. Sprouse, and R. Surman, “Coproduction of Light and Heavy r -process Elements via Fission Deposition,” *The Astrophysical Journal* **896**, 28 (2020), 1911.07766.
- [7] B. Côté, C. L. Fryer, K. Belczynski, O. Korobkin, M. Chruślińska, N. Vassh, M. R. Mumpower, J. Lippuner, T. M. Sprouse, R. Surman, and R. Wollaeger, “The Origin of r -process Elements in the Milky Way,” *The Astrophysical Journal* **855**, 99 (2018), 1710.05875.
- [8] J. Sadhukhan, W. Nazarewicz, and N. Schunck, “Microscopic modeling of mass and charge distributions in the spontaneous fission of ^{240}Pu ,” *Phys. Rev. C* **93**, 011304 (2016).
- [9] A. J. Sierk, “Langevin model of low-energy fission,” *Phys. Rev. C* **96**, 034603 (2017).
- [10] M. D. Usang, F. A. Ivanyuk, C. Ishizuka, and S. Chiba, “Correlated transitions in TKE and mass distributions of fission fragments described by 4-D Langevin equation,” *Sci. Rep.* **9**, 1525 (2019).
- [11] C. Simenel and A. S. Umar, “Heavy-ion collisions and fission dynamics with the time-dependent Hartree-Fock theory and its extensions,” *Prog. Part. Nucl. Phys.* **103**, 19–66 (2018).
- [12] G. Scamps, C. Simenel, and D. Lacroix, “Dynamical description of the fission process using the TD-BCS theory,” *AIP Conf. Proc.* **1681**, 040003 (2015).
- [13] A. Bulgac, S. Jin, K. J. Roche, N. Schunck, and I. Stetcu, “Fission dynamics of ^{240}Pu from saddle to scission and beyond,” *Phys. Rev. C* **100**, 034615 (2019).
- [14] A. Bulgac, S. Jin, and I. Stetcu, “Unitary evolution with fluctuations and dissipation,” *Phys. Rev. C* **100**, 014615 (2019).
- [15] D. Regnier, N. Dubray, and N. Schunck, “From asymmetric to symmetric fission in the fermion isotopes within the time-dependent generator-coordinate-method formalism,” *Phys. Rev. C* **99**, 024611 (2019).
- [16] J. Zhao, J. Xiang, Z.-P. Li, T. Nikšić, D. Vretenar, and S.-G. Zhou, “Time-dependent generator-coordinate-method study of mass-asymmetric fission of actinides,” *Phys. Rev. C* **99**, 054613 (2019).
- [17] K.-H. Schmidt and B. Jurado, “Review on the progress in nuclear fission—experimental methods and theoretical descriptions,” *Rep. Prog. Phys.* **81**, 106301 (2018).
- [18] J. Randrup, P. Möller, and A. J. Sierk, “Fission-fragment mass distributions from strongly damped shape evolution,” *Phys. Rev. C* **84**, 034613 (2011).
- [19] P. Möller and T. Ichikawa, “A method to calculate fission-fragment yields $Y(Z,N)$ versus proton and neutron number in the brownian shape-motion model,” *Eur. Phys. J. A* **51**, 173 (2015).
- [20] M. R. Mumpower, P. Jaffke, M. Verriere, and J. Randrup, “Primary fission fragment mass yields across the chart of nuclides,” (2019), arXiv:1911.06344 [nucl-th].
- [21] P. Fong, “Asymmetric fission,” *Phys. Rev.* **89**, 332–333 (1953).
- [22] E. Erba, U. Facchini, and E. Saetta-Menichella, “Statistical analysis of low-energy fission,” *Nucl. Phys.* **84**, 595–608 (1966).
- [23] B. D. Wilkins, E. P. Steinberg, and R. R. Chasman, “Scission-point model of nuclear fission based on deformed-shell effects,” *Phys. Rev. C* **14**, 1832–1863 (1976).
- [24] J.-F. Lemaître, S. Panebianco, J.-L. Sida, S. Hilaire, and S. Heinrich, “New statistical scission-point model to predict fission fragment observables,” *Phys. Rev. C* **92**, 034617 (2015).
- [25] J.-F. Lemaître, S. Goriely, S. Hilaire, and J.-L. Sida, “Fully microscopic scission-point model to predict fission fragment observables,” *Phys. Rev. C* **99**, 034612 (2019).
- [26] A. V. Andreev, G. G. Adamian, N. V. Antonenko, S. P. Ivanova, S. N. Kuklin, and W. Scheid, “Ternary fission within statistical approach,” *Eur. Phys. J. A* **30**, 579–589 (2006).
- [27] H. Paşca, A. V. Andreev, G. G. Adamian, and N. V. Antonenko, “Change of the shape of mass and charge distributions in fission of cf isotopes with excitation energy,” *Phys. Rev. C* **99**, 064611 (2019).
- [28] U. Brosa and S. Grossmann, “In the exit channel of nuclear fission,” *Z. Phys. A* **310**, 177–187 (1983).
- [29] S. Oberstedt, F.-J. Hampsch, and F. Vivès, “Fission-mode calculations for ^{239}U , a revision of the multi-modal random neck-rupture model,” *Nucl. Phys. A* **644**, 289–305 (1998).
- [30] K.-H. Schmidt, B. Jurado, C. Amouroux, and C. Schmitt, “General description of fission observables: GEF model code,” *Nucl. Data Sheets* **131**, 107–221 (2016).
- [31] A. Kelić, M. V. Ricciardi, and K.-H. Schmidt, “ABLA07 - towards a complete description of the decay channels of a nuclear system from spontaneous fission to multifrag-

- mentation,” (2009), [arXiv:0906.4193 \[nucl-th\]](https://arxiv.org/abs/0906.4193).
- [32] J. d. J. Mendoza-Temis, M.-R. Wu, K. Langanke, G. Martínez-Pinedo, A. Bauswein, and H.-T. Janka, “Nuclear robustness of the r process in neutron-star mergers,” *Phys. Rev. C* **92**, 055805 (2015).
- [33] S. Goriely and G. Martínez Pinedo, “The production of transuranium elements by the r-process nucleosynthesis,” *Nucl. Phys. A* **944**, 158–176 (2015).
- [34] J. Sadhukhan, C. Zhang, W. Nazarewicz, and N. Schunck, “Formation and distribution of fragments in the spontaneous fission of ^{240}Pu ,” *Phys. Rev. C* **96**, 061301 (2017).
- [35] Z. Matheson, S. A. Giuliani, W. Nazarewicz, J. Sadhukhan, and N. Schunck, “Cluster radioactivity of ^{294}Og ,” *Phys. Rev. C* **99**, 041304 (2019).
- [36] J. W. Negele, “Microscopic theory of fission dynamics,” *Nucl. Phys. A* **502**, 371 – 386 (1989).
- [37] W. Nazarewicz, “Diabaticity of nuclear motion: problems and perspectives,” *Nucl. Phys. A* **557**, 489–514 (1993).
- [38] J. Sadhukhan, K. Mazurek, A. Baran, J. Dobaczewski, W. Nazarewicz, and J. A. Sheikh, “Spontaneous fission lifetimes from the minimization of self-consistent collective action,” *Phys. Rev. C* **88**, 064314 (2013).
- [39] G. Scamps and C. Simenel, “Impact of pear-shaped fission fragments on mass-asymmetric fission in actinides,” *Nature* **564**, 382–385 (2018).
- [40] V. Strutinsky and A. Magner, “The semiclassical theory of the shell structure of the nucleus,” *Sov. J. Part. Nucl.* **7**, 459 (1976).
- [41] K. ichiro Arita, T. Ichikawa, and K. Matsuyanagi, “Semiclassical origin of asymmetric nuclear fission: nascent-fragment shell effect in periodic-orbit theory,” *Phys. Scr.* **95**, 024003 (2020).
- [42] J. Bondorf, A. Botvina, A. Iljinov, I. Mishustin, and K. Snepken, “Statistical multifragmentation of nuclei,” *Phys. Rep.* **257**, 133 – 221 (1995).
- [43] C. Simenel and A. S. Umar, “Formation and dynamics of fission fragments,” *Phys. Rev. C* **89**, 031601 (2014).
- [44] U. Mosel and H. Schmitt, “Potential energy surfaces for heavy nuclei in the two-center model,” *Nucl. Phys. A* **165**, 73 – 96 (1971).
- [45] A. Staszczak, A. Baran, J. Dobaczewski, and W. Nazarewicz, “Microscopic description of complex nuclear decay: Multimodal fission,” *Phys. Rev. C* **80**, 014309 (2009).
- [46] N. Schunck, J. Dobaczewski, W. Satuła, P. Bączyk, J. Dudek, Y. Gao, M. Konieczka, K. Sato, Y. Shi, X. Wang, and T. Werner, “Solution of the Skyrme-Hartree-Fock-Bogolyubov equations in the Cartesian deformed harmonic-oscillator basis. (VIII) HFODD (v2.73y): A new version of the program,” *Comput. Phys. Commun.* **216**, 145–174 (2017).
- [47] J. Bartel, P. Quentin, M. Brack, C. Guet, and H.-B. Håkansson, “Towards a better parametrisation of Skyrme-like effective forces: A critical study of the SkM force,” *Nucl. Phys. A* **386**, 79–100 (1982).
- [48] N. Schunck, J. D. McDonnell, J. Sarich, S. M. Wild, and D. Higdon, “Error analysis in nuclear density functional theory,” *J. Phys. G* **42**, 034024 (2015).
- [49] J. Dobaczewski, W. Nazarewicz, and M. Stoitsov, “Nuclear ground-state properties from mean-field calculations,” *Eur. Phys. J. A* **15**, 21–26 (2002).
- [50] J. C. Pei, W. Nazarewicz, J. A. Sheikh, and A. K. Ker-
man, “Fission barriers of compound superheavy nuclei,” *Phys. Rev. Lett.* **102**, 192501 (2009).
- [51] V. Martin and L. M. Robledo, “Fission barriers at finite temperature: A theoretical description with the Gogny force,” *Int. J. Mod. Phys. E* **18**, 861–868 (2009).
- [52] N. Schunck, D. Duke, and H. Carr, “Description of induced nuclear fission with skyrme energy functionals. ii. finite temperature effects,” *Phys. Rev. C* **91**, 034327 (2015).
- [53] P.-G. Reinhard, J. A. Maruhn, A. S. Umar, and V. E. Oberacker, “Localization in light nuclei,” *Phys. Rev. C* **83**, 034312 (2011).
- [54] C. L. Zhang, B. Schuetrumpf, and W. Nazarewicz, “Nucleon localization and fragment formation in nuclear fission,” *Phys. Rev. C* **94**, 064323 (2016).
- [55] W. D. Myers and W. J. Swiatecki, “Nuclear masses and deformations,” *Nucl. Phys.* **81**, 1 – 60 (1966).
- [56] M. Warda, A. Staszczak, and W. Nazarewicz, “Fission modes of mercury isotopes,” *Phys. Rev. C* **86**, 024601 (2012).
- [57] I. Tsekhanovich, A. Andreyev, K. Nishio, D. Denis-Petit, K. Hirose, H. Makii, Z. Matheson, K. Morimoto, K. Morita, W. Nazarewicz, R. Orlandi, J. Sadhukhan, T. Tanaka, M. Vermeulen, and M. Warda, “Observation of the competing fission modes in ^{178}Pt ,” *Phys. Lett. B* **790**, 583–588 (2019).
- [58] E. K. Hulet, J. F. Wild, R. J. Dougan, R. W. Lougheed, J. H. Landrum, A. D. Dougan, P. A. Baisden, C. M. Henderson, R. J. Dupzyk, R. L. Hahn, M. Schädel, K. Sümmerer, and G. R. Bethune, “Spontaneous fission properties of ^{258}Fm , ^{259}Md , ^{260}Md , ^{258}No , and ^{260}No : Bimodal fission,” *Phys. Rev. C* **40**, 770–784 (1989).
- [59] P. Möller, J. Nix, and W. Swiatecki, “New developments in the calculation of heavy-element fission barriers,” *Nucl. Phys. A* **492**, 349 – 387 (1989).
- [60] U. Brosa, S. Grossmann, and A. Müller, “Nuclear scission,” *Phys. Rep.* **197**, 167 – 262 (1990).
- [61] J. Sadhukhan, J. Dobaczewski, W. Nazarewicz, J. A. Sheikh, and A. Baran, “Pairing-induced speedup of nuclear spontaneous fission,” *Phys. Rev. C* **90**, 061304 (2014).
- [62] J. Zhao, B.-N. Lu, T. Nikšić, and D. Vretenar, “Multidimensionally constrained relativistic Hartree-Bogoliubov study of spontaneous nuclear fission,” *Phys. Rev. C* **92**, 064315 (2015).
- [63] A. Baran, J. A. Sheikh, J. Dobaczewski, W. Nazarewicz, and A. Staszczak, “Quadrupole collective inertia in nuclear fission: Cranking approximation,” *Phys. Rev. C* **84**, 054321 (2011).
- [64] S. A. Giuliani and L. M. Robledo, “Non-perturbative collective inertias for fission: A comparative study,” *Phys. Lett. B* **787**, 134–140 (2018).
- [65] L. Moretto and R. Babinet, “Large superfluidity enhancement in the penetration of the fission barrier,” *Phys. Lett. B* **49**, 147 – 149 (1974).
- [66] R. Bernard, S. A. Giuliani, and L. M. Robledo, “Role of dynamic pairing correlations in fission dynamics,” *Phys. Rev. C* **99**, 064301 (2019).
- [67] G. Scamps and C. Simenel, “Effect of shell structure on the fission of sub-lead nuclei,” *Phys. Rev. C* **100**, 041602 (2019).
- [68] J. Laidler and F. Brown, “Mass distribution in the spontaneous fission of ^{240}Pu ,” *J. Inorg. Nucl. Chem.* **24**, 1485–1492 (1962).

- [69] R. Brandt, S. G. Thompson, R. C. Gatti, and L. Phillips, “Mass and energy distributions in the spontaneous fission of some heavy isotopes,” *Phys. Rev.* **131**, 2617–2624 (1963).
- [70] J. E. Gindler, K. F. Flynn, L. E. Glendenin, and R. K. Sjoblom, “Distribution of mass, kinetic energy, and neutron yield in the spontaneous fission of ^{257}Fm ,” *Phys. Rev. C* **16**, 1483–1492 (1977).
- [71] R. M. Harbour, K. W. MacMurdo, D. E. Troutner, and M. V. Hoehn, “Mass and nuclear charge distributions from the spontaneous fission of ^{254}Fm ,” *Phys. Rev. C* **8**, 1488–1493 (1973).
- [72] K. F. Flynn, E. P. Horwitz, C. A. A. Bloomquist, R. F. Barnes, R. K. Sjoblom, P. R. Fields, and L. E. Glendenin, “Distribution of mass in the spontaneous fission of ^{256}Fm ,” *Phys. Rev. C* **5**, 1725–1729 (1972).
- [73] D. C. Hoffman, J. B. Wilhelmy, J. Weber, W. R. Daniels, E. K. Hulet, R. W. Lougheed, J. H. Landrum, J. F. Wild, and R. J. Dupzyk, “12.3-min ^{256}Cf and 43-min ^{258}Md and systematics of the spontaneous fission properties of heavy nuclides,” *Phys. Rev. C* **21**, 972–981 (1980).
- [74] C. Schmitt, A. Guessous, J. Bocquet, H.-G. Clerc, R. Brissot, D. Engelhardt, H. Faust, F. Gönnerwein, M. Mutterer, H. Nifenecker, J. Pannicke, C. Ristori, and J. Theobald, “Fission yields at different fission-product kinetic energies for thermal-neutron-induced fission of ^{239}Pu ,” *Nucl. Phys. A* **430**, 21 – 60 (1984).
- [75] K. F. Flynn, J. E. Gindler, R. K. Sjoblom, and L. E. Glendenin, “Mass distributions for thermal-neutron-induced fission of ^{255}Fm and ^{251}Cf ,” *Phys. Rev. C* **11**, 1676–1680 (1975).
- [76] K.-H. Schmidt, A. Kelić, and M. V. Ricciardi, “Experimental evidence for the separability of compound-nucleus and fragment properties in fission,” *Europhys. Lett.* **83**, 32001 (2008).
- [77] S. Goriely, S. Hilaire, A. J. Koning, M. Sin, and R. Capote, “Towards a prediction of fission cross sections on the basis of microscopic nuclear inputs,” *Phys. Rev. C* **79**, 024612 (2009).
- [78] J. Erler, K. Langanke, H. P. Loens, G. Martínez-Pinedo, and P.-G. Reinhard, “Fission properties for r-process nuclei,” *Phys. Rev. C* **85**, 25802 (2012).
- [79] S. A. Giuliani, G. Martínez-Pinedo, and L. M. Robledo, “Fission properties of superheavy nuclei for r-process calculations,” *Phys. Rev. C* **97**, 034323 (2018).
- [80] S. A. Giuliani, G. Martínez-Pinedo, M. R. Wu, and L. M. Robledo, “Fission and the r-process nucleosynthesis of translead nuclei,” (2019), [arXiv:1904.03733 \[nucl-th\]](https://arxiv.org/abs/1904.03733).
- [81] F. Gönnerwein, “Even-odd effects of fragment yields in low energy fission,” *Phys. Procedia* **47**, 107 – 114 (2013).